Journal of Earth Science, *Vol. 28*, *No. 1*, *p. 078–091*, *February 2017* *ISSN 1674-487X*
Printed in China
DOI: 10.1007/s12583-017-0739-3

A High Temperature and High Pressure Experimental Study on Re-Bearing Capability of Sulfide

Yingying Liu[1], **Zhilong Huang***[1], **Chengming Zhu**[2]
1. *State Key Laboratory of Ore Deposit Geochemistry*, *Institute of Geochemistry*, *Chinese Academy of Sciences*, *Guiyang* 550002, *China*
2. *Key Laboratory for High Temperature & High Pressure Study of the Earth's Interior*, *Institute of Geochemistry*, *Chinese Academy of Sciences*, *Guiyang* 550002, *China*
Yingying Liu: http://orcid-org/0000-0003-2656-2514; Zhilong Huang: http://orcid-org/0000-0002-4062-5107

ABSTRACT: High temperature (1 270–1 550 ºC) and high pressure (1.0 GPa) experimental studies on Re-bearing capabilities of pyrite, galena and sphalerite from typical Pb-Zn ore deposits were performed on a six-anvil apparatus. We observed microstructures of the quenched sulfides using scanning electron microscope (SEM) and analyzed compositions of the run products using both energy disperse spectroscopy (EDS) and electron probe microanalyzer (EPMA). The results show that pyrite melt can dissolve much more metallic Re than galena and sphalerite melts, forming scattered acicular ReS_2 in the quenched matrix of pyrrhotite ($Fe_{1-x}S$). The quenched matrixes of $Fe_{1-x}S$, PbS and ZnS generally contain less than 1.0 wt.% of Re and their Re-bearing capabilities seem to range as $Fe_{1-x}S$>PbS>ZnS. However, Re partition coefficients between them are difficult to estimate, because Re distribution is inhomogeneous in the quenched sulfide matrixes.
KEY WORDS: pyrite, galena, sphalerite, high P-T experiment, Re-bearing capability.

0 INTRODUCTION

^{187}Re-^{187}Os isotope system is an effective tool for geochemical study of the earth and planetary evolution. Both Re and Os are siderophile elements mostly enriched in alloy and sulfide phases. As Os is a highly compatible element during partial melting of mantle and Re is a moderately incompatible element (Brenan, 2008; Sattari et al., 2002), the crust has much higher Re/Os ratios (~50; Esser and Turekian, 1993) than the mantle (<0.4; Meisel et al., 1996). This significant geochemical behavior makes ^{187}Re-^{187}Os isotope system available for tracing and dating.

High parent isotope content is essential for establishing a radioisotope system. Thus, concentration of ^{187}Re is a key to application of ^{187}Re-^{187}Os isotope system. For example, molybdenite can contain ~4.21 wt.% (Melfos et al., 2001) of Re, and has a high Re-Os isotopic closure temperature as ~500 ºC (Selby and Creaser, 2004; Barra et al., 2003; Stein et al., 2001; Suzuki et al., 1996). Thus, molybdenite Re-Os isotope chronometry is successfully utilized to date different hydrothermal ore deposits (Fu et al., 2016; Hu et al., 2016; Liu et al., 2012; Song et al., 2012; Zeng et al., 2012; Feng et al., 2011; Li W C et al., 2011; Liu et al., 2011; Wang et al., 2011; Xie et al., 2011; Lentz and Suzuki, 2000) and other geological studies (Li N et al., 2011; Li W C et al., 2011; Gao et al., 2010; Dai et al., 2009; Taghipour et al., 2008; Zimmerman et al., 2008; Lu et al., 2006; Barra et al., 2005; Zeng et al., 2004). However, molybdenites contain variable contents of Re (Berzina et al., 2005; Mao et al., 1999), which can be as high as ~4.21 wt.% (Melfos et al., 2001), or as low as 4.8 ng/g–5.0 μg/g (Chen et al., 2006; Stein, 2006). Other sulfides also have variable concentrations of Re, which can be as high as 538 ng/g (Li N et al., 2011), or as low as 0.094 ng/g (Freydier et al., 1997). Previous studies indicate that the high Re-Os budget in sulfides is not controlled by microintergrowths of molybdenite (Selby et al., 2009; Berzina et al., 2005), but related to organic-bearing rocks (Huang et al., 2013b). However, what controls the wide variation of Re in sulfides is still unknown.

Paragenetic phenomenon of sulfides is normal in hydrothermal and magmatic deposits. Pyrite, pyrrhotite and arsenopyrite are always associated with each other in epithermal gold deposit (Morelli et al., 2010, 2005; Yu et al., 2005; Arne et al., 2001). Chalcopyrite, bornite, pyrite and molybdenite are also commonly intergrown in sedimentary rock-hosted stratiform copper deposits (Huang et al., 2013b; Zhu and Sun, 2013; Chen and Zhou, 2012). In skarn deposits, sphalerite and galena are always associated with molybdenite, pyrite, chalcopyrite and pyrrhotite (Liu et al., 2012; Song et al., 2012; Xie et al., 2011; Lentz and Suzuki, 2000). In magmatic Ni-Cu sulfide deposits, pyrrhotite are closely associated with pentlandite and chalcopyrite (Lü et al., 2011).

Low concentrations (pg/g~ng/g) of Re and Os in sulfide also can be well determined for Re-Os dating with the development of analytical methods (Qi et al., 2013, 2010;

*Corresponding author: huangzhilong@vip.gyig.ac.cn

Manuscript received September 17, 2015.
Manuscript accepted December 2, 2015.

Liu, Y. Y., Huang, Z. L., Zhu, C. M., 2017. A High Temperature and High Pressure Experimental Study on Re-Bearing Capability of Sulfide. *Journal of Earth Science*, 28(1): 78–91. doi:10.1007/s12583-017-0739-3. http://en.earth-science.net

Reisberg and Meisel, 2002; Meisel et al., 2001), which greatly enlarge the application field of sulfide Re-Os dating (Liu et al., 2015; Li N et al., 2011; Zhang et al., 2011; Kelley et al., 2010; Morelli et al., 2010, 2005, 2004; Nozaki et al., 2010; Feng et al., 2009; Selby et al., 2009; Yu et al., 2005; Mathur et al., 2002, 2000, 1999; Arne et al., 2001; Kirk et al., 2001; Stein et al., 2000). From previous studies, concentrations of Re are 3–5 orders of magnitude higher in molybdenites than in paragenetic pyrites (Li N et al., 2011; Barra et al., 2003) or chalcopyrites (Zhu and Sun, 2013; Chen and Zhou, 2012). In some deposits, Re is 3–30 times more concentrated in pyrites than in sphalerites (Morelli et al., 2004; Liu Yingying unpub. data) or galenas (Stein et al., 2000), and sphalerites have significant higher concentration of Re than galenas (Liu et al., 2015). These might be resulted from the distribution coefficients of Re between different sulfides, which are related to the Re-bearing capabilities of these sulfides. However, in other deposits the variation of Re between pyrite, sphalerite and galena is not obvious (Spry et al., 2014; Levresse et al., 2004). The varied concentrations of Re, Os and Re/Os ratios in hydrothermal sulfides is always explained as heterogeneity of Re and Os in the ore-forming fluid (Huang et al., 2013a; Morelli et al., 2004; Freydier et al., 1997). In magmatic system, Re and Os contents are controlled by original Re and Os compositions of the melts and the distribution coefficients (Righter et al., 1998). This is also applicable in the hydrothermal system (Huang et al., 2014; Berzina et al., 2005). Therefore, it is difficult to distinguish whether the varied concentrations of Re among different sulfides result from inhomogenous of the ore-forming fluid or different distribution coefficients. Re-bearing capability of different sulfides is key to the problem and has to be studied further. The distribution pattern of Re among different sulfides is significant to application of their Re-Os isotope system.

Solubility of Re and Os is previously studied in silicate melt (Bennett and Brenan, 2013; Ertel et al., 2001), FeS sulfide melt (Fonseca et al., 2011, 2007), and hydrothermal fluid (Xiong et al., 2006; Xiong and Wood, 2002, 2001, 1999). Studies on the distribution coefficients of Re and Os in silicate/sulfide melts are also ongoing (Buono et al., 2013, Mallmann and O'Neill, 2007; Brenan, 2002; Sattari et al., 2002; Righter et al., 1998). However, the distribution and diffusion characters of Re and Os between different sulfides (Brenan et al., 2000) so far have not received any adequate attentions.

Pyrite, galena and sphalerite are the major ore minerals in Pb-Zn sulfide ore deposits and are usually associated with each other. Re-Os isotope systems of these sulfides would provide important information for ore genesis. Therefore, we firstly choose these three sulfides to conduct high P-T experiments and compare their Re-bearing capabilities based on SEM observations of the quenched samples and analytical results of both energy disperse spectrum (EDS) and electron probe microanalyzer (EPMA). This study provides theoretical foundation on distribution of Re in Pb-Zn ore deposit and is applicable to similar studies on solubility of Re and/or other metals (e.g. platinum group elements) in sulfide melts.

1 EXPERIMENTAL AND ANALYTICAL METHODS

1.1 Starting Materials

Sulfide samples used in this study are selected from typical Pb-Zn ore deposits and have low concentrations of Re<1.0 ng/g. Pyrite and sphalerite are from the Laochang Pb-Zn deposit in Lancang, Yunnan Province (Ye et al., 2012), and galena is from the Fule Pb-Zn deposit, Yunnan Province (Si, 2006). The Pb-Zn ore samples were mechanically crushed and washed by Milli-Q water. After sieved to 20–40 meshes, pyrite, galena and sphalerite separates were sorted by hand-picking under a binocular microscope with >99% degree of purity. The separates were further pulverized in an agate mortar to fine powders of >200 meshes. The X-ray powder diffraction (XRD; D/max-2200) analysis results of the separates are shown in Fig. 1. The pyrite and sphalerite have high degree of purity, while the galena still contains a little Zn, even though it is pure enough from the naked eye. The XRD results of the galena have good reproducibility (Figs. 1c, 1d; Liu et al., 2015).

The metallic slice of Re (99.9%) was made in Germany with thickness of 0.01 mm and was processed to Re belts in size of 2 mm×50 mm for the high P-T experiments.

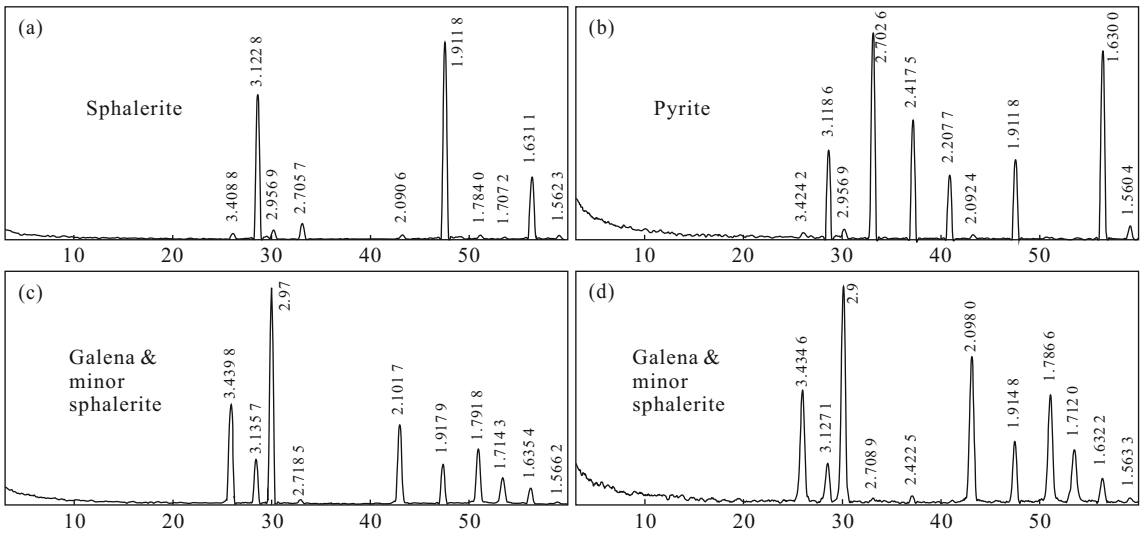

Figure 1. X-ray diffraction results of sulfide samples. (c) and (d) are replicate determinations of the galena powder.

1.2 Temperature and Pressure Conditions

Previous studies on solubility of Re and Os in silicate melt are normally conducted through high temperature (1 400–2 300 ºC) and high pressure (0.1 MPa–2 GPa) experiments (Bennett and Brenan, 2013; Ertel et al., 2001), while studies of sulfide melt are usually under high temperature (1 200–1 400 ºC) and ordinary pressure experiments (Pruseth et al., 2014; Fonseca et al., 2011, 2007). Therefore, to ensure attainment of equilibration, the experimental duration of sulfide melts should be as long as 24–96 h, which is time-consuming. Regardless of the high pressure effect, this study merely uses the fast reaction kinetics in sulfide melts under high pressure conditions to dissolve the metallic Re as soon as possible. Therefore, the experimental pressure is fixed at 1.0 GPa, which is proved available (Table 1).

Because FeS_2 would decompose to FeS+S during heating (Stevens et al., 2005), the composition of the quenched melt produced by the melting of pyrite is no longer FeS_2, but monosulfide of $Fe_{1-x}S$ (pyrrhotite) which is proved by EPMA results (Table 2). Melting points of pyrrhotite, galena and sphalerite are separately 1 192, 1 114 and 1 670 ºC under ordinary pressure (Sharp, 1969), while melting point of metallic Re is as high as 3 180 ºC. When the pressure increases to 1.0 GPa, the melting points would also increase. Therefore, the initial experimental temperatures for pyrite, galena and sphalerite are separately set at 1 270, 1 350 and 1 480 ºC. Detailed conditions of the experiments are listed in Table 1.

1.3 Experimental Procedure

All the experiments in this paper were performed using the DS 3600 T/6 six-anvil apparatus equipped at the Key Laboratory for High Temperature & High Pressure Study of the Earth's Interior, Institute of Geochemistry, Chinese Academy of Sciences. The upper limit of temperature and pressure was 2 000 ºC and 7.0 GPa. The starting materials were loaded in a graphite capsule with 6 mm in length and 6 mm inner diameter. The folded Re belt was laid flat in the center of the capsule (Fig. 2a). The sulfide powder was cold-pressed to pressures higher than 100 MPa. The loaded capsule was set in a thin-walled (1 mm) hexagonal boron nitride (HBN) sleeve, with two HBN caps at both ends. The HBN sleeve was then placed in a graphite heater, which was sandwiched by two calcined pyrophyllite disks at both ends. It was then further fixed in the graphite heater by two pyrophyllite tapers at both ends. The detailed sample assemblage for the experiments is shown in Fig. 2b. The temperature was measured and controlled using $PtRh_6$-$PtRh_{30}$ thermocouple which was protected by HBN tubes (Fig. 2b). The temperature error is within 5 ºC. Long-term monitoring results on the six-anvil apparatus (Fu and Zhu, 1985) show that the temperature gradient in the sample chamber is about 6 ºC. The pressure error is within 0.2 MPa. In a single run, the sample was first pressed and then heated to the desired conditions. After annealing at the experimental conditions, we quenched the sample by cutting off the power. The recovered sample was mounted in epoxy, and cut parallel to the heater axis. EDS and EPMA were used for analysis of Re.

1.4 Sample Analysis

The surface morphology observation and chemistry configuration of the sulfide melt were initially conducted on the JSM-6460-(LV) type scanning electron microscopy (SEM) with EDS at the State Key Laboratory of Environmental Geochemistry, Institute of Geochemistry, Chinese Academy of Sciences. The accelerating voltage was 25 kV, and the working distance was 12 mm. The electron beam diameter was 60 nm (10^{-2} μm). The results are shown in Figs. 3–6 and Table 1.

The Re, Fe, Pb, Zn, S, As and Cu compositions of different phases in the run products were measured by a JXA-8100 electron microprobe at the State Key Laboratory of Lithospheric Evolution, Institute of Geology and Geophysics, Chinese Academy of Sciences. The instrument was operated at a beam current of 20 nA and an accelerating voltage of 20 kV. The beam was defocused to a spot size of 3 μm. Well defined natural sulfide minerals and synthetic metals were used as standards. Re was measured with Mα lines and the spectral overlap interferences from Pb were well subtracted. The detection limit of Re is approximately 250 ppm and all the analytical results are listed in Table 2.

2 EXPERIMENTAL RESULTS

2.1 High P-T Experimental Results

All the high P-T experiments went well without any explosions and the recovered samples show good reproducibility on pyrite, sphalerite and galena (Table 1; Fig. 3). Thus, the experiments on these sulfides can retain safety under conditions of 1 480 ºC and 1.0 GPa. The representative backscattered

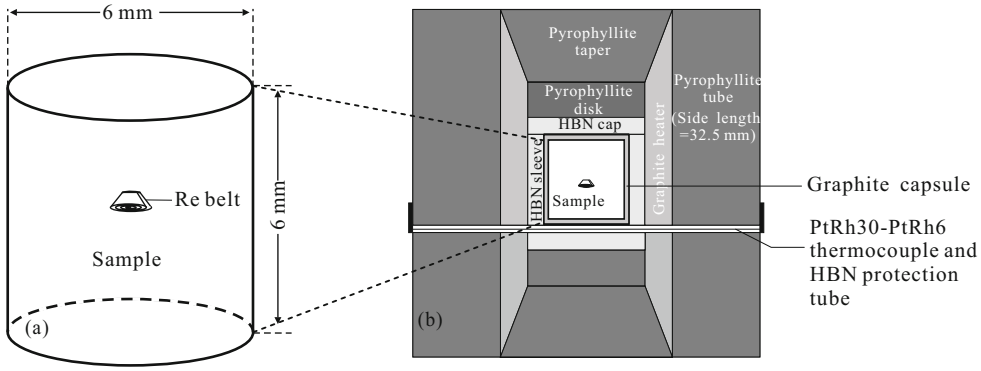

Figure 2. Diagrams showing the sample assemblage for the experiments in this study. (a) The cylinder samples and Re belt; (b) the assembly of high temperature and pressure experiment (modified from Zhang et al., 2015).

Table 1 Experimental conditions and EDS analysis results of the run products

Run	Sample	Temperature (ºC)	Duration (h)	Matrix	Residual Re belt (%)※	Run products	Arisen sequence of the run products	Images	Descriptions
1	Pyrite & Re	1 270	0.5	$Fe_{1-x}S$	~10%	$Fe_{1-x}S$, ReS_2, Re	ReS_2>$Fe_{1-x}S$	Fig. 3a	(1) Residual Re belt fallen to the bottom of cylinder; (2) Acicular ReS_2 scattered in the matrix
2	Pyrite & Re	1 380	0.5	$Fe_{1-x}S$	<1%	$Fe_{1-x}S$, ReS_2	ReS_2>$Fe_{1-x}S$	Figs. 3b–3c; Figs. 4a–4c	(1) Acicular ReS_2 scattered in the matrix; (2) Little metallic Re remained in the matrix
3	Pyrite & Re	1 480	0.5	$Fe_{1-x}S$	<1%	$Fe_{1-x}S$, ReS_2	ReS_2>$Fe_{1-x}S$	Figs. 3d–3e	
4	Pyrite & Re	1 380	2.0	$Fe_{1-x}S$	<1%	$Fe_{1-x}S$, ReS_2	ReS_2>$Fe_{1-x}S$	Figs. 3f, 4f–4j	
5	Pyrite & Re	1 380	4.0	$Fe_{1-x}S$	<1%	$Fe_{1-x}S$, ReS_2	ReS_2>$Fe_{1-x}S$	Figs. 3g, 4d, 4e	(1) Acicular ReS_2 scattered in the matrix; (2) Little metallic Re remained in the matrix; (3) Cumulates of ReS_2 formed at the bottom of the cylinder
6	*Pyrite & Galena & Re	1 480	0.5	PbS & $Fe_{1-x}S$	<1%	PbS, $Fe_{1-x}S$, ReS_2	ReS_2>$Fe_{1-x}S$>PbS	Figs. 3k, 4k–4n	(1) Acicular ReS_2 scattered in the matrix; (2) Little metallic Re remained in the matrix; (3) PbS distributed in the cranny and clearance of $Fe_{1-x}S$
7	Galena & Re	1 350	0.5	PbS & ZnS	~80%	PbS, ZnS, Re	ZnS>PbS	Figs. 3h	(1) Metallic Re belt remained in the matrix and has fallen to the bottom of cylinder; (2) Fine-grained ZnS widely distributed
8	Galena & Re	1 450	0.5	PbS & ZnS	~80%	PbS, ZnS, Re	ZnS>PbS	Figs. 5f–5i	
9	Galena & Re	1 380	2.0	PbS & ZnS	~80%	PbS, ZnS, Re	ZnS>PbS	Figs. 3i, 5a–5e	
10	Galena & Re	1 380	4.0	PbS & ZnS	~80%	PbS, ZnS, Re	ZnS>PbS	Figs. 3j, 5j–5l	
11	Sphalerite & Re	1 480	0.5	ZnS & PbS	~90%	ZnS, PbS, Re	ZnS>PbS	Figs. 3l, 6a–6d	(1) Metallic Re belt remained in the matrix and has fallen to the bottom of cylinder; (2) PbS distribute in the cranny and clearance of ZnS
12	Sphalerite & Re	1 550	0.5	ZnS & PbS	~90%	ZnS, PbS, Re	ZnS>PbS	Figs. 6l–6o	
13	Sphalerite & Re	1 480	2.0	ZnS & PbS	~90%	ZnS, PbS, Re	ZnS>PbS	Figs. 3m–3n, 6e–6k	(1) Metallic Re belt remained in the matrix and has fallen to the bottom of cylinder; (2) Residual melt ($Fe_{1-x}S$/PbS) distributed in the cranny and clearance of ZnS; (3) Recrystallization phenomenon are seen at edge of the Re belt and the folded Re belt
14	Sphalerite & Re	1 480	4.0	ZnS & PbS	~90%	ZnS, PbS, Re	ZnS>PbS	Figs. 3o	

※. The percentage of residual Re belt is from visual estimation; *. the pyrite and galena are separately around 50%.

Table 2 EPMA data (wt.%) of different phases in the run products

Spot	Matrix	Condition	Phase	Re	As	Fe	S	Cu	Pb	Zn	Total	S/Re*	S/Fe*	S/Pb*	S/Zn*
1	Pyrite	1 380 °C, 2.0 h	$Fe_{1-x}S$	0.33	0.00	57.80	39.07	0.07	0.32	0.10	97.69		1.18		
2	Pyrite	1 380 °C, 2.0 h	$Fe_{1-x}S$	0.69	0.01	57.48	38.98	0.11	0.31	0.13	97.72		1.18		
3	Pyrite	1 380 °C, 2.0 h	$Fe_{1-x}S$	0.48	0.00	57.20	39.09	0.08	0.17	0.11	97.12		1.19		
4	Pyrite	1 380 °C, 2.0 h	Acicular ReS_2	73.18	0.00	2.21	22.12	0.00	0.13	0.00	97.64	1.76			
5	Pyrite	1 380 °C, 4.0 h	$Fe_{1-x}S$	0.36	0.01	57.68	38.88	0.09	0.25	0.10	97.38		1.17		
6	Pyrite	1 380 °C, 4.0 h	$Fe_{1-x}S$	0.32	0.00	57.36	39.16	0.11	0.19	0.12	97.45		1.19		
7	Pyrite	1 380 °C, 4.0 h	$Fe_{1-x}S$	0.59	0.00	57.76	39.15	0.12	0.30	0.11	98.04		1.18		
8	Pyrite	1 380 °C, 4.0 h	Accumulated ReS_2	75.96	0.00	0.14	22.52	0.01	0.08	0.00	98.71	1.72			
9	Galena	1 380 °C, 2.0 h	PbS	0.10	0.02	0.18	13.59	0.01	83.40	1.81	99.11			1.05	
10	Galena	1 380 °C, 2.0 h	ZnS	0.06	0.03	0.45	31.78	0.00	3.66	61.86	97.83				1.05
11	Galena	1 380 °C, 2.0 h	PbS	0.77	0.00	0.13	13.77	0.04	84.18	1.71	100.59			1.06	
12	Galena	1 380 °C, 2.0 h	ZnS	0.26	0.00	0.44	32.00	0.01	2.40	62.33	97.44				1.05
13	Galena	1 380 °C, 4.0 h	PbS	0.26	0.01	0.13	13.54	0.01	83.98	0.51	98.43			1.04	
14	Galena	1 380 °C, 4.0 h	ZnS	0.21	0.00	0.47	32.46	0.00	1.84	62.75	97.72				1.05
15	Galena	1 380 °C, 4.0 h	PbS	0.04	0.00	0.49	14.86	0.03	79.50	5.92	100.83			1.21	
16	Galena	1 380 °C, 4.0 h	ZnS	0.25	0.00	0.43	32.29	0.01	1.81	62.88	97.67				1.05
17	Sphalerite	1 480 °C, 2.0 h	ZnS	0.00	0.00	5.57	32.92	0.05	0.39	60.17	99.09				1.11
18	Sphalerite	1 480 °C, 2.0 h	ZnS	0.86	0.00	5.50	33.41	0.05	0.35	50.07	98.24				1.17
19	Sphalerite	1 480 °C, 2.0 h	Residual melt	0.00	0.10	9.81	23.41	0.19	49.33	17.21	100.05				
20	Sphalerite	1 480 °C, 2.0 h	Re belt	98.51	0.00	0.02	0.09	0.00	0.13	0.00	98.82				
21[✱]	Sphalerite	1 480 °C, 4.0 h	ZnS	0.12	0.00	6.40	32.96	0.05	0.20	59.63	99.35				1.13
22[✱]	Sphalerite	1 480 °C, 4.0 h	ZnS	0.07	0.00	6.84	33.12	0.08	0.21	59.06	99.38				1.14
23[✱]	Sphalerite	1 480 °C, 4.0 h	ZnS	0.00	0.00	5.51	33.08	0.07	0.38	60.63	99.67				1.11
24	Sphalerite	1 480 °C, 4.0 h	ZnS	0.44	0.00	7.39	33.55	0.07	0.35	56.53	98.33				1.21
25	Sphalerite	1 480 °C, 4.0 h	Residual melt	0.00	0.02	13.33	29.09	0.35	20.65	37.28	100.72				

*. Stoichiometric ratios calculated from atom (%) results of EPMA; [✱]. spots 21–23 are from the places adjacent to the Re belt same as spots H–J shown in Fig. 6e; Spot 21 is the nearest to Re belt and Spot 23 is the farthest.

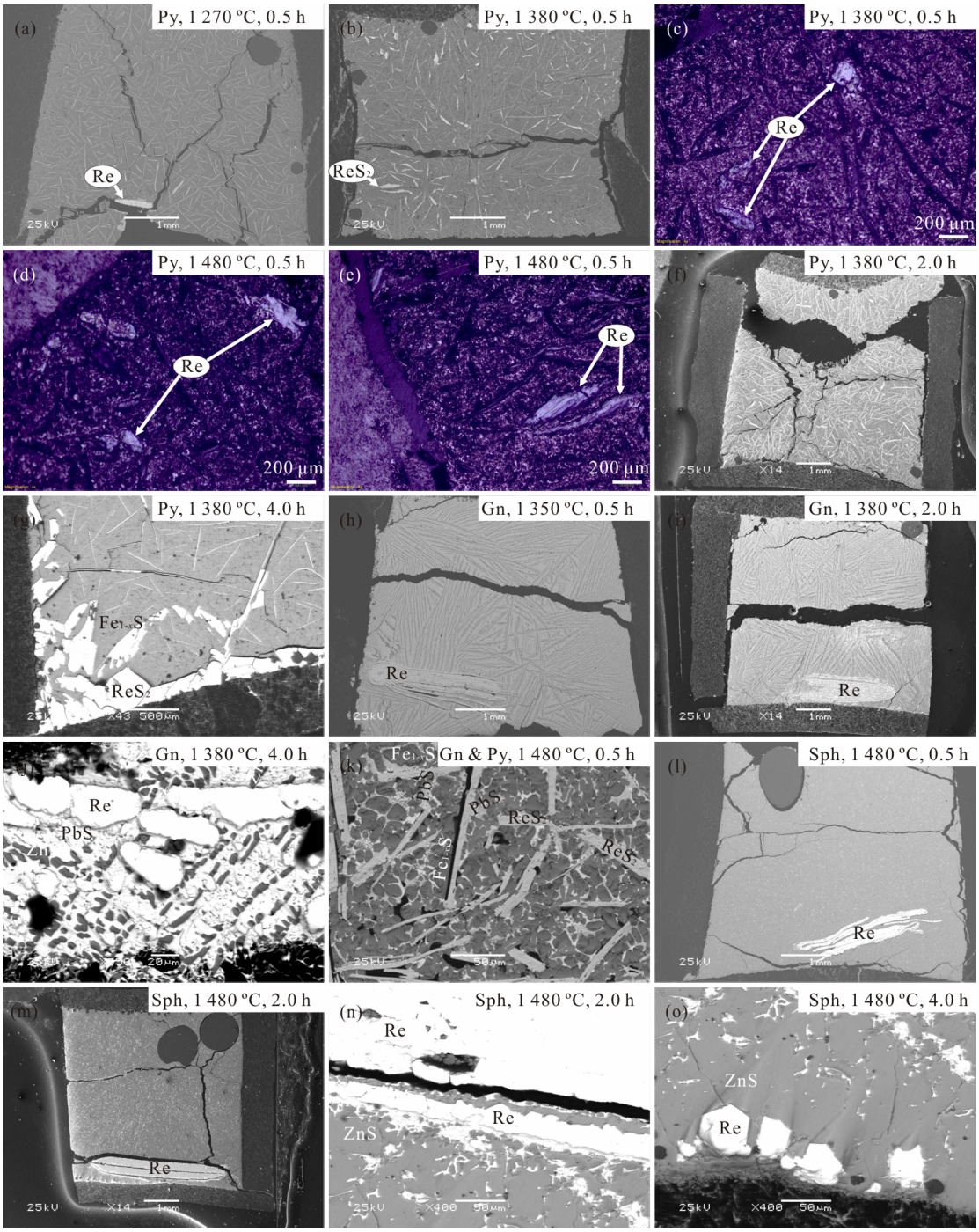

Figure 3. Representative photos of run products. (a) BSE image of pyrite melt after heated at 1 270 ºC for 0.5 h. Residual metallic Re belt has fallen to the bottom of cylinder. Scattered ReS_2 was formed in the quenched melt. (b) BSE image of pyrite melt after heated at 1 380 ºC for 0.5 h. Little metallic Re remained and scattered ReS_2 was formed in the quenched melt. (c)–(e) Microscope photos of pyrite melt after heated at 1 380–1 480 ºC for 0.5 h. Undissolved fine metallic Re remained in the melt. (f) BSE image of pyrite melt after heated at 1 380 ºC for 2.0 h. Little metallic Re remained and scattered ReS_2 was formed in the quenched melt. (g) BSE image of pyrite melt after heated at 1 380 ºC for 4.0 h. Little metallic Re remained in the melt. Cumulates of ReS_2 was formed at the bottom of the pyrite cylinder. (h) BSE image of galena melt after heated at 1 350 ºC for 0.5 h. Metallic Re belt remained in the melt and has fallen to the bottom of cylinder. Flow structure consisting of ZnS grains was widely developed in the quenched melt. (i) BSE image of galena melt after heated at 1 350 ºC for 2.0 h. Metallic Re belt remained in the melt and has fallen to the bottom of cylinder. Flow structure consisting of ZnS grains was widely developed. (j) BSE image of galena melt after heated at 1 350 ºC for 4.0 h. Undissoved metallic Re belt was corroded. (k) BSE image of a mixed matrix consisting of pyrite (~50%) and galena (~50%) after heated at 1480 ºC for 0.5 h. Little metallic Re remained and scattered ReS_2 was widely distributed in the quenched melt. The sulfide melt differentiated strongly. The early-formed $Fe_{1-x}S$ was surrounded by the later-formed PbS. (l) BSE image of sphalerite melt after heated at 1 480 ºC for 0.5 h. Metallic Re belt remained in the melt and has fallen to the bottom of cylinder. (m) BSE image of galena melt after heated at 1 480 ºC for 2.0 h. Metallic Re belt remained in the melt and has fallen to the bottom of cylinder. (n)–(o) BSE images of galena melt after heated at 1 480 ºC for 2.0–4.0 h. Recrystallization phenomena are observed at the edge of the Re belt. Py. Pyrite; Gn. galena; Sph. sphalerite.

electron (BSE) images are shown in Figs. 3–6. These SEM-BSE images clearly show typical textures of quenched eutectic melts (Figs. 3–6).

Abundant acicular rhenium sulfides (ReS_2) formed in pyrite melt (Figs. 3a, 3b; Table 2), which is different from galena and sphalerite melts. We initially added metallic Re into the pyrite matrix, but it turns out to be ReS_2 (Table 2) after undergoing the high P-T conditions. The sulfur that reacted with Re should have come from pyrite (FeS_2), thus, the pyrite matrix cannot avoid sulfur (as S_2) loss during the experiments and

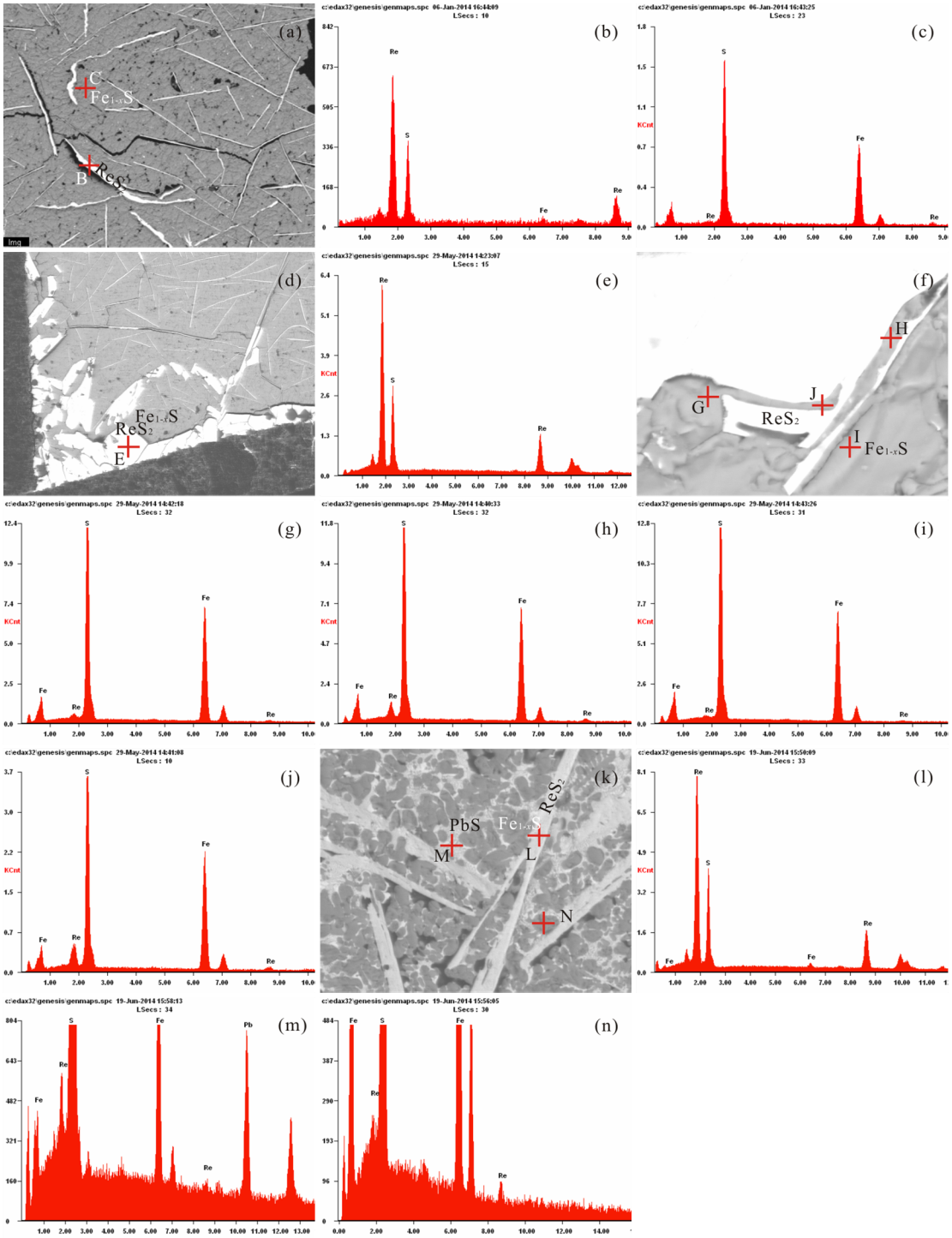

Figure 4. Energy disperse spectroscopy results of high temperature high pressure experiment products in pyrite melt. (a) BSE image of pyrite melt after heated at 1 380 ºC for 0.5 h. (b) Energy spectra of B. The scattered spicula consist of ReS_2. (c) Energy spectra of C. Re is detectable in the quenching melt of pyrite. (d) BSE image of pyrite melt after heated at 1 380 ºC for 4.0 h. (e) Energy spectra of E. Cumulates of ReS_2 formed at the bottom of the cylinder. (f) BSE image of pyrite melt after heated at 1 380 ºC for 2.0 h. (g)–(j) Energy spectra of G–J. Re is detectable in the quenching melt of pyrite. (k) BSE image of the mixed melt of pyrite (~50%) and galena (~50%) after heated at 1 480 ºC for 0.5 h. (l) Energy spectra of L. The scattered spicula also consist of ReS_2. (m) Energy spectra of L. PbS in the matrix is detectable of Re. (n) Energy spectra of L. $Fe_{1-x}S$ in the matrix is detectable of Re.

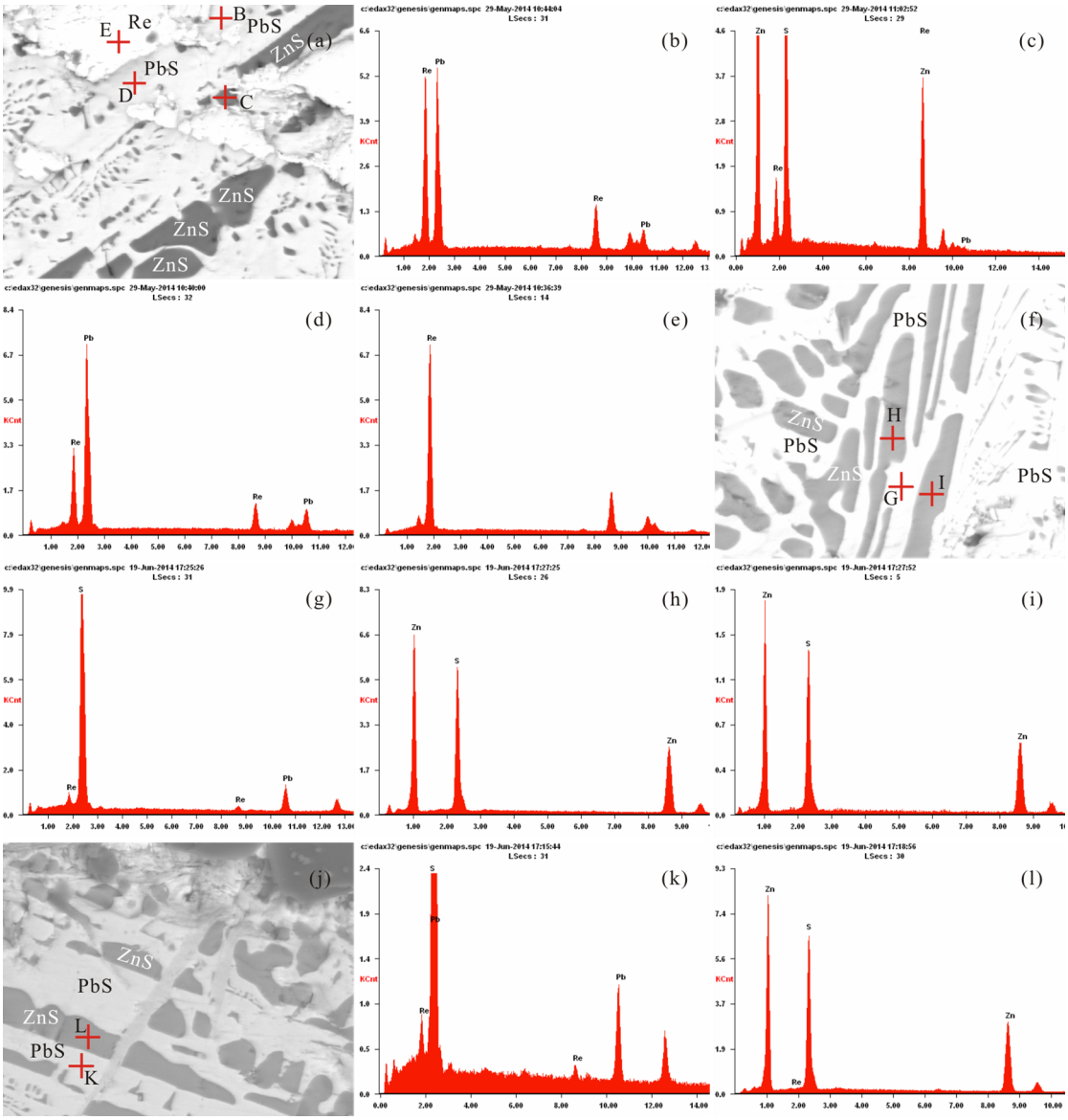

Figure 5. Energy disperse spectroscopy results of high temperature high pressure experiment products in galena melt. (a) BSE image of galena melt after heated at 1 380 ºC for 2.0 h; (b) energy spectra of B, PbS in the matrix is detectable of Re; (c) energy spectra of C, some ZnS in the matrix is detectable of Re; (d) energy spectra of D, PbS in the matrix is detectable of Re; and (e) energy spectra of E, residual metallic Re is eroded in galena melt; (f) BSE image of galena melt after heated at 1 350 ºC for 0.5 h; (g) energy spectra of G, PbS in the matrix is detectable of Re, (h)–(i) energy spectra of H–I, some ZnS in the matrix is undetectable of Re; (j) BSE image of galena melt after heated at 1 380 ºC for 4.0 h; (k) energy spectra of K, PbS in the matrix is detectable of Re; (l) energy spectra of L, some ZnS in the matrix is undetectable of Re.

composition of the matrix turns to monosulfide ($Fe_{1-x}S$) which is proved by EPMA results (Table 2). In Run 1 (Table 1), the original folded Re belt still could be observed in the $Fe_{1-x}S$ matrix after annealing at 1 270 ºC for 0.5 h (Fig. 3 a). In runs 2–3, when the $Fe_{1-x}S$ matrix annealed at 1 380 and 1 480 ºC for 0.5 h, the original Re belt nearly disappeared (Figs. 3c, 3d, 3e). In runs 4–5, when the duration increased to 2.0–4.0 h, Re was completely dissolved (Fig. 3f).

As indicated in Run 6, the mixed melt consisting of pyrite (~50%) and galena (~50%) can also dissolve metallic Re completely at 1.0 GPa and 1 480 ºC after 0.5 h, forming scattered acicular ReS_2 in the melt (Fig. 3k). However, the quenched melt of Run 6 differentiated strongly (Figs. 4k–4n). The void space among grains of $Fe_{1-x}S$ is filled with PbS (Figs. 4k–4n). Quenched galena (runs 7–10) and sphalerite melts (runs 11–14) also differentiated. The run products of galena were characterized by presence of graphic textures and quenched melt patches (Figs. 3h–3j). The first-solidified ZnS grains are fine and widely scattered in the PbS matrix. In the quenched sphalerite melt, void space among grains of ZnS is filled with the residual melt of $Fe_{1-x}S$/PbS (Figs. 6l–6o; Table 2). In the galena and sphalerite melts, the metallic Re belt was only partly dissolved under the varied durations of 0.5–4.0 h, and the residual Re has dropped to the bottom of the sample cylinder (Figs. 3h, 3i, 3l, 3m). Densities of pyrite, galena and sphalerite are separately 5.0, 7.6 and 4.1 g/cm^3, while that of metallic Re is 21.0 g/cm^3. Therefore, the fallen Re belt could indicate that the sulfide had reached molten state during the high P-T conditions. Thus, under 1.0 GPa, the

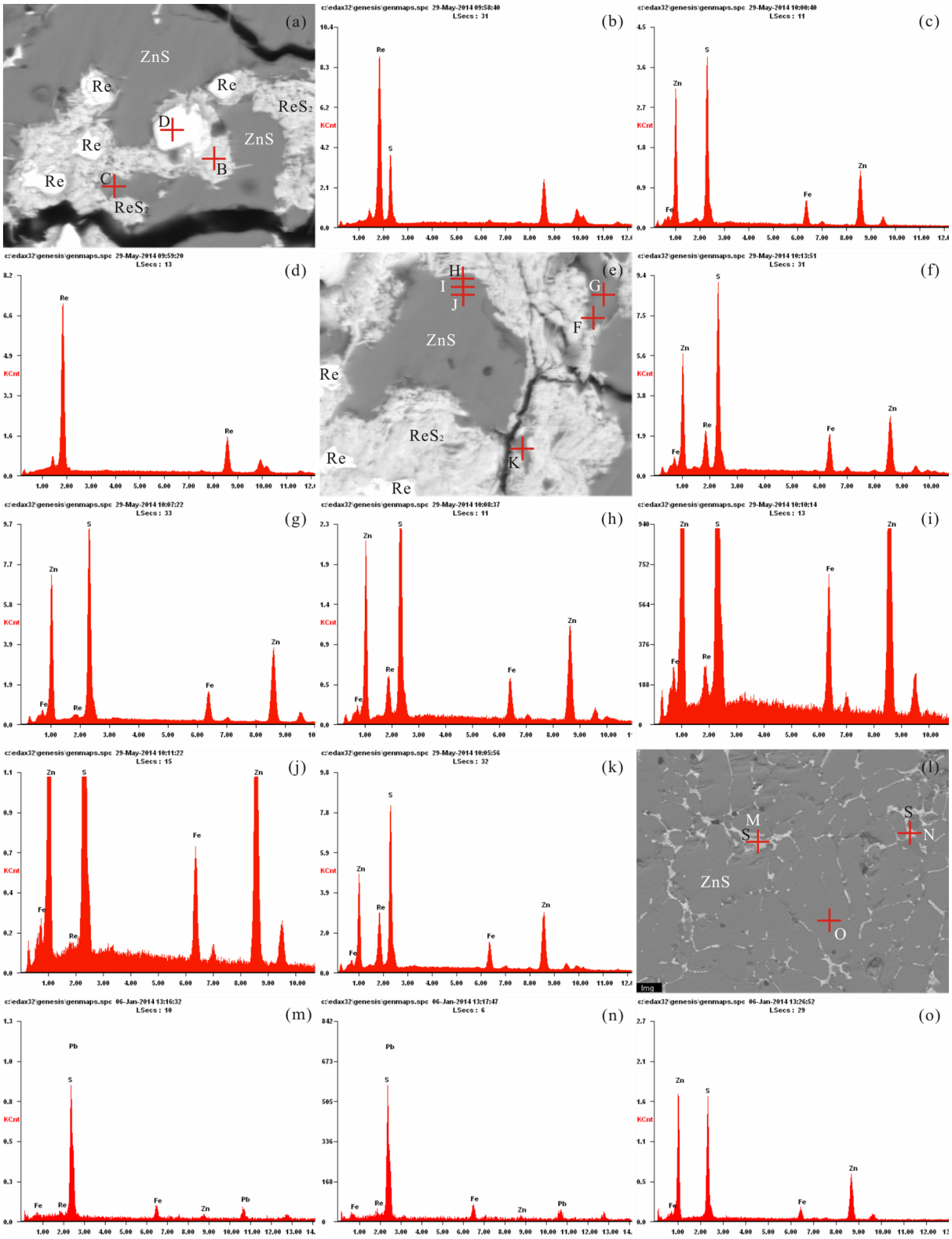

Figure 6. Energy disperse spectroscopy results of high temperature high pressure experiment products in sphalerite melt. (a) BSE image of sphalerite melt after heated at 1 480 ºC for 0.5 h; (b) energy spectra of B, ReS_2 formed in the sphalerite melt; (c) energy spectra of C, signal of Re is weak in some ZnS of the melt; (d) energy spectra of D, eroded grained metallic Re which is wrapped by ReS_2 formed in the sphalerite melt; (e) BSE image of pyrite melt after heated at 1 480 ºC for 2.0 h; (f) energy spectra of F, Re is detectable in ZnS matrix and signal of Re is strong in ZnS which is near to ReS_2; (g) energy spectra of G, signal of Re is weaker in ZnS which is farther away from ReS_2 than spot 'F'; (h) energy spectra of H, signal of Re is strong in ZnS which is near to ReS_2; (i) energy spectra of I, signal of Re is a little weaker in ZnS which is farther away from ReS_2 than spot 'H'; (j) energy spectra of J, signal of Re is weak in ZnS which is far away from ReS_2; (k) energy spectra of K, signal of Re is strong in ZnS which is near to ReS_2; (l) BSE image of pyrite melt after heated at 1 480 ºC for 4.0 h;, (m)–(n) energy spectra of M–N, PbS distributed in the cranny and clearance of ZnS is detectable of Re; (o) energy spectra of O, ZnS is nearly undetectable of Re.

powdered pyrite, galena and sphalerite were molten at temperatures of 1 270, 1 350 and 1 480 ºC, respectively, after annealing for 0.5 h. The folded Re belts were conglutinated under high P-T conditions (Figs. 3a, 3h, 3i, 3l, 3m), and were partly broken and corroded (Figs. 3j, 5a, 6a, 6e).

2.2 EDS and EPMA Results

Re is detectable in all the quenched matrixes of $Fe_{1-x}S$ (Fig. 4), galena (Fig. 5) and sphalerite (Fig. 6) by EDS and the results are shown in Figs. 4–6.

Corrected EPMA results are shown in Table 2. The S/Fe stoichiometric ratios of pyrite (FeS_2) melt are much lower than 2.0 with an average of 1.18, which proves that pyrite melt has lost some sulfur and turns out to be $Fe_{1-x}S$. The S/Re stoichiometric ratio of the acicular and accumulated rhenium sulfides formed in pyrite melt is around 1.74, which is close to 2.0. Thus, the composition is likely to be ReS_2. The stoichiometric ratios of both S/Zn and S/Pb in the ZnS and PbS matrixes are still around 1.0. In pyrite melt concentration of Re range from 0.32 wt.%–0.69 wt.% in the matrix of $Fe_{1-x}S$. In the galena melt the first-solified ZnS grains contain 0.06 wt.%–0.26 wt.% of Re, while the matrix of PbS contains 0.04 wt.%–0.77 wt.% of Re. In the sphalerite melt, contents of Re vary between 0.00 wt.%–0.86 wt.% in the matrix of ZnS, while concentrations of Re in the residual melt is only 0.00 wt.%.

3 DISCUSSION

3.1 Duration

As indicated in runs 2–5, little metallic Re remains in the pyrite melts of 1 380 and 1 480 ºC after annealing for 0.5 h (Figs. 3c–3e; Table 1), thus, the duration of 0.5 h is long enough to melt the pyrite matrix. After annealing for 2.0–4.0 h, the Re belt was dissolved completely, and ReS_2 crystals began to accumulate at the bottom of the pyrite cylinder (Fig. 3g). It seems that if the duration is longer than 4.0 h, there would accumulate more ReS_2 at the bottom of pyrite cylinder. However, as indicated in runs 7–10 and runs 11–14, the concentrations of Re in the galena and sphalerite melts did not increase with the longer annealing durations (Figs. 5, 6). In runs 13 and 14, when the duration reached 2.0–4.0 h, cumulates of metallic Re were presented at the bottom of sphalerite cylinder (Figs. 3n–3o). Thus, from this set of experiments, duration of 2.0 h is long enough for the sulfide melts and metallic Re to attain kinetic equilibrium. The metallic Re might be recrystallized after annealing for 2.0 h. As shown in Fig. 3n, the original smooth Re belt became rough and crystal edges were observed. In Fig. 3o, even the crystallized grains of metallic Re are seen at the bottom of sphalerite cylinder.

3.2 Temperature

Under 1.0 GPa, the pyrite melt at 1 270 ºC cannot dissolve metallic Re completely in 0.5 h, leaving some original folded metallic Re at the bottom (Fig. 3a). However, when the temperature increases to 1 380 and 1 480 ºC, the pyrite melts can dissolve metallic Re completely, forming scattered ReS_2 in the matrix (Figs. 3b, 3f). Thus, temperature can influence the solubility of Re in sulfide melt.

As pyrite, galena and sphalerite powders can stably melt at 1 350–1 480 ºC and 1.0 GPa without any explosions, the Re-bearing capabilities of these sulfide melts can be compared under this condition. At 1 350–1 480 ºC and 1.0 GPa, the pyrite melt (Figs. 3b–3g) can dissolve more Re than galena (Figs. 3h, 3i) and sphalerite (Figs. 3l, 3m) melts. Neither galena melt nor sphalerite melt can dissolve Re completely even when the temperature increased to 1 480 ºC at 1.0 GPa (Figs. 3l, 3m). Thus, temperature is not the key factor for dissolving of Re in galena and sphalerite melts.

From the quantitative data of EPMA shown in Table 2, the Re-bearing capabilities of the sulfide matrixes can be compared under the above P-T condition and seem to range as $Fe_{1-x}S$>PbS>ZnS.

3.3 Fugacity of S_2 (fS_2)

Re is a moderately incompatible element. The high-temperature geochemical behaviors of Re range from chalcophile for reduced MORB-type mantle (Fonseca et al., 2007) to strongly lithophile for highly oxidized island-arc melts (Mallmann and O'Neill, 2007). Re is chalcophile in sulfide melts. The solubility of Re always increases with increasing fS_2 (Fonseca et al., 2011, 2007; Brenan, 2008) or sulfur content (Buono et al., 2013; Fonseca et al., 2009; Sattari et al., 2002).

The experimental results of Run 10 (Table 1) indicated that once pyrite exists in the matrix, the dissolving of Re increase significantly (Figs. 3k, 4k–4n). As pyrite (FeS_2) contains much more sulfur than galena (PbS) and sphalerite (ZnS), and breakdown of pyrite (FeS_2) to pyrrhotite ($Fe_{1-x}S$) simultaneously with the appearance of free sulfur (Sharp, 1969), which would increase the fugacity of S_2 (fS_2). Dissolving of metallic Re seems to be affected by fS_2, which is very similar to the previous conclusions (Fonseca et al., 2011, 2007; Brenan, 2008). However, our EPMA results show that concentrations of Re in quenched matrix of $Fe_{1-x}S$ are only slightly higher than PbS and ZnS (Table 2). Thus, the dissolved Re in pyrite melt might dominantly exist in forms of ReS_2, rather than in lattice of $Fe_{1-x}S$ matrix.

3.4 Differentiation of Sulfide Melt

Published researches have proposed that some metamorphosed massive sulfide deposits (including the Broken Hill deposit, Australia) have partially melted (Spry et al., 2008; Huston et al., 2006). To verify whether or not the Pb-Zn deposit has experienced the melting process, researchers studied melting behavior of the PbS-FeS-ZnS-(S) system (Stevens et al., 2005; Mavrogenes et al., 2001), finding that at 1 atm the eutectic temperature of system PbS-FeS-ZnS is ~800 ºC. Due to the solidus-lowering effect of additional components (Pruseth et al., 2014; Frost et al., 2002; Mavrogenes et al., 2001), realistic volcanogenic massive sulfide or SEDEX sulfide compositions would melt at a lower temperature (<600 °C). The presence of a sulfur-rich fluid phase may even promote melting during high-grade metamorphism (Stevens et al., 2005). If the sulfides contain proper amount of Re, once the molten sulfide quenched or differentiated, Re would redistribute among different sulfide phases.

In this study, from the paragenetic relationship of sulfide phases in the quenched samples (Figs. 4k–4n, 3h–3j, 6l–6o),

ZnS, $Fe_{x-1}S$ and PbS solidified successively, which is consistent with their melting points (1 670, 1 192 and 1 114 ºC). In galena melt, the residual melt of PbS seems to have higher concentrations of Re than the first-solifidied ZnS (Figs. 5a–5e; Table 2). In sphalerite melt, the first-solidified ZnS is hardly detectable of Re by EDS, while the residual melt is detectable of Re (Figs. 6l–6o). However, the quantitative EPMA data showed that concentrations of Re in the residual melt are even slightly lower than ZnS in sphalerite melt (Table 2). This might due to the inhomogeneous distribution of Re in the sulfide matrix. The inhomogeneous distribution of Re is also supported by the phenomena that signals of Re are stronger in the spots near ReS_2 or metallic Re, the farther the weaker (Figs. 4f–4j, 6e–6k; Table 2). Thus, Re partition coefficients between different sulfide phases are difficult to estimate in this study.

Pyrite, sphalerite and galena melts can dissolve an appropriate amount of Re through high P-T conditions, and Re is detectable in all matrixes of $Fe_{1-x}S$, PbS and ZnS. However, the distribution coefficients of Re between these phases are undetermined due to the inhomogeneous distribution of Re in the sulfide melts even after duration of 4.0 h (Table 2). Thus, the detailed geochemical manner of Re and whether the differentiation of the quenched sulfide melt would fractionate Re and influence the distribution of Re still need further investigations.

4 CONCLUSIONS

(1) Under 1.0 GPa, powders of natural pyrite, galena and sphalerite can reach molten state after separately annealing at temperatures of 1 270, 1 350 and 1 480 ºC for 0.5 h. These sulfide melts have the ability to dissolve metallic Re.

(2) Pyrite (FeS_2) melt can dissolve much more metallic Re than galena (PbS) and sphalerite (ZnS) melts, forming scattered acicular ReS_2 in the quenched matrix. The Re-bearing capability of these sulfide minerals seems related to fS_2.

(3) Run products of pyrite, galena and sphalerite quenched from 1.0 GPa & 1 350–1 480 ºC after annealing for 2.0–4.0 h are available for Re-bearing capability study. Re-bearing capabilities of these quenched sulfide matrixes seem to range as $Fe_{1-x}S$>PbS>ZnS. However, Re differentiation coefficients between the sulfide phases are undetermined due to the inhomogeneous distribution of Re, which remains to be further studied.

ACKNOWLEDGMENTS

This study was supported by the National Natural Science Foundation of China (No. 41430315) and the National Basic Research Program of China (No. 2014CB440905). Thanks are given to Dr. Mingliang Wang for useful discussions and suggestions. Comments and suggestions from three anonymous reviewers greatly improved the quality of this paper. The final publication is available at Springer via http://dx.doi.org/10.1007/s12583-017-0739-3.

REFERENCES CITED

Arne, D. C., Bierlein, F. P., Morgan, J. W., et al., 2001. Re-Os Dating of Sulfides Associated with Gold Mineralization in Central Victoria, Australia. *Economic Geology*, 96(6): 1455–1459. doi:10.2113/gsecongeo.96.6.1455

Barra, F., Ruiz, J., Mathur, R., et al., 2003. A Re-Os Study of Sulfide Minerals from the Bagdad Porphyry Cu-Mo Deposit, Northern Arizona, USA. *Mineralium Deposita*, 38(5): 585–596. doi:10.1007/s00126-002-0341-0

Barra, F., Ruiz, J., Valencia, V. A., et al., 2005. Laramide Porphyry Cu-Mo Mineralization in Northern Mexico: Age Constraints from Re-Os Geochronology in Molybdenite. *Economic Geology*, 100(8): 1605–1616. doi:10.2113/gsecongeo.100.8.1605

Bennett, N. R., Brenan, J. M., 2013. Controls on the Solubility of Rhenium in Silicate Melt: Implications for the Osmium Isotopic Composition of Earth's Mantle. *Earth and Planetary Science Letters*, 361: 320–332. doi:10.1016/j.epsl.2012.10.028

Berzina, A. N., Sotnikov, V. I., Economou-Eliopoulos, M., et al., 2005. Distribution of Rhenium in Molybdenite from Porphyry Cu-Mo and Mo-Cu Deposits of Russia (Siberia) and Mongolia. *Ore Geology Reviews*, 26(1/2): 91–113. doi:10.1016/j.oregeorev.2004.12.002

Brenan, J. M., 2002. Re-Os Fractionation in Magmatic Sulfide Melt by Monosulfide Solid Solution. *Earth and Planetary Science Letters*, 199(3/4): 257–268. doi:10.1016/s0012-821x(02)00581-2

Brenan, J. M., 2008. Re-Os Fractionation by Sulfide Melt-Silicate Melt Partitioning: A New Spin. *Chemical Geology*, 248(3/4): 140–165. doi:10.1016/j.chemgeo.2007.09.003

Brenan, J. M., Cherniak, D. J., Rose, L. A., 2000. Diffusion of Osmium in Pyrrhotite and Pyrite: Implications for Closure of the Re-Os Isotopic System. *Earth and Planetary Science Letters*, 180(3/4): 399–413. doi:10.1016/s0012-821x(00)00165-5

Buono, S. S., Dasgupta, R., Lee, C. A., et al., 2013. Siderophile Element Partitioning between Cohenite and Liquid in the Fe-Ni-S-C System and Implications for Geochemistry of Planetary Cores and Mantles. *Geochimica et Cosmochimica Acta*, 120: 239–250. doi:10.1016/j.gca.2013.06.024

Chen, W. T., Zhou, M. F., 2012. Paragenesis, Stable Isotopes, and Molybdenite Re-Os Isotope Age of the Lala Iron-Copper Deposit, Southwest China. *Economic Geology*, 107(3): 459–480. doi:10.2113/econgeo.107.3.459

Chen, Z. H., Wang, D. H., Qu, W. J., et al., 2006. Geological Characteristics and Mineralization Age of the Taoxikeng Tungsten Deposit in Chongyi County, Southern Jiangxi Province, China. *Geological Bulletin of China*, 25(4): 496–501 (in Chinese with English Abstract)

Dai, J. Z., Mao, J. W., Zhao, C. S., et al., 2009. New U-Pb and Re-Os Age Data and the Geodynamic Setting of the Xiaojiayingzi Mo (Fe) Deposit, Western Liaoning Province, Northeastern China. *Ore Geology Reviews*, 35(2): 235–244. doi:10.1016/j.oregeorev.2008.10.001

Ertel, W., O'Neill, H. S., Sylvester, P. J., 2001. The Solubility of Rhenium in Silicate Melts: Implications for the Geochemical Properties of Rhenium at High Temperatures. *Geochemica et Cosmochimica Acta*, 65(13): 2161–2170. doi:10.1016/s0016-7037(01)00582-8

Esser, B. K., Turekian, K. K., 1993. The Osmium Isotopic Composition of the Continental Crust. *Geochimica et Cosmochimica Acta*, 57(13): 3093–3104.

doi:10.1016/0016-7037(93)90296-9

Feng, C. Y., Qu, W. J., Zhang, D. Q., et al., 2009. Re-Os Dating of Pyrite from the Tuolugou Stratabound Co(Au) Deposit, Eastern Kunlun Orogenic Belt, Northwestern China. *Ore Geology Reviews*, 36(1–3): 213–220. doi:10.1016/j.oregeorev.2008.10.005

Feng, C. Y., Zeng, Z. L., Zhang, D. Q., et al., 2011. SHRIMP Zircon U-Pb and Molybdenite Re-Os Isotopic Dating of the Tungsten Deposits in the Tianmenshan-Hongtaoling W-Sn Orefield, Southern Jiangxi Province, China, and Geological Implications. *Ore Geology Reviews*, 43(1): 8–25. doi:10.1016/j.oregeorev.2011.04.006

Fonseca, R. O. C., Campbell, I. H., O'Neill, H. S. C., et al., 2009. Solubility of Pt in Sulphide Mattes: Implications for the Genesis of PGE-Rich Horizons in Layered Intrusions. *Geochimica et Cosmochimica Acta*, 73(19): 5764–5777. doi:10.1016/j.gca.2009.06.038

Fonseca, R. O. C., Mallmann, G., O'Neill, H. S. C., et al., 2007. How Chalcophile is Rhenium? An Experimental Study of the Solubility of Re in Sulphide Mattes. *Earth and Planetary Science Letters*, 260(3/4): 537–548. doi:10.1016/j.epsl.2007.06.012

Fonseca, R. O. C., Mallmann, G., O'Neill, H. S. C., et al., 2011. Solubility of Os and Ir in Sulfide Melt: Implications for Re/Os Fractionation during Mantle Melting. *Earth and Planetary Science Letters*, 311(3/4): 339–350. doi:10.1016/j.epsl.2011.09.035

Freydier, C., Ruiz, J., Chesley, J., et al., 1997. Re-Os Isotope Systematics of Sulfides from Felsic Igneous Rocks: Application to Base Metal Porphyry Mineralization in Chile. *Geology*, 25(9): 775. doi:10.1130/0091-7613(1997)025<0775:roisos>2.3.co;2

Frost, B. R., Mavrogenes, J. A., Tomkins, A. G., 2002. Partial Melting of Sulfide Ore Deposits during Medium- and High-Grade Metamorphism. *The Canadian Mineralogist*, 40(1): 1–18. doi:10.2113/gscanmin.40.1.1

Fu, H. F., Zhu, C. M., 1985. High Pressure Fusion Curve of Alloys $Ni_{70}Mn_{30}$, $Ni_{40}Mn_{30}Fe_{30}$ and $Ni_{70}Mn_{25}Co_5$ Used in Synthesizing Diamonds. *Journal of Chinese Silicate Solicate*, 13: 381–384 (in Chinese)

Fu, Y., Dong, L., Li, C., et al., 2016. New Re-Os Isotopic Constrains on the Formation of the Metalliferous Deposits of the Lower Cambrian Niutitang Formation. *Journal of Earth Science*, 27(2): 271–281. doi:10.1007/s12583-016-0606-7

Gao, Y., Li, Y. F., Guo, B. J., et al., 2010. Geological Characteristics and Molybdenite Re-Os Isotopic Dating of Qianfanling Quartz-Vein Mo Deposit in Songxian County, Western Henan Province. *Acta Petrologica Sinica*, 26(3): 757–767 (in Chinese with English Abstract)

Hu, K. M., Tang, Z. C., Meng, X. S., et al., 2016. Chronology of Petrogenesis and Mineralization of Datongkeng Porphyry W-Mo Deposit in West Zhejiang. *Earth Science*, 41(9): 1435–1450 (in Chinese with English Abstract)

Huang, X. W., Qi, L., Gao, J. F., et al., 2013a. First Reliable Re-Os Ages of Pyrite and Stable Isotope Compositions of Fe(-Cu) Deposits in the Hami Region, Eastern Tianshan Orogenic Belt, NW China. *Resource Geology*, 63(2): 166–187. doi:10.1111/rge.12003

Huang, X. W., Zhao, X. F., Qi, L., 2013b. Re-Os and S Isotopic Constraints on the Origins of Two Mineralization Events at the Tangdan Sedimentary Rock-Hosted Stratiform Cu Deposit, SW China. *Chemical Geology*, 347: 9–19. doi:10.1016/j.chemgeo.2013.03.020

Huang, X. W., Qi, L., Wang, Y. C., et al., 2014. Re-Os Dating of Magnetite from the Shaquanzi Fe-Cu Deposit, Eastern Tianshan, NW China. *Science China*: *Earth Sciences*, 57(2): 267–277. doi:10.1007/s11430-013-4660-z

Huston, D. L., Stevens, B., Southgate, P. N., et al., 2006. Australian Zn-Pb-Ag Ore-Forming Systems: A Review and Analysis. *Economic Geology*, 101(6): 1117–1157. doi:10.2113/gsecongeo.101.6.1117

Kelley, K. D., Slack, J. F., Selby, D., et al., 2010. Geochemistry and Geochronology of Carbonate-Hosted Base Metal Deposits in the Southern Brooks Range, Alaska: Temporal Link to VMS Deposits and Metallogenic Implications. James Cook Univ., Townsville. 454–456

Kirk, J., Ruiz, J., Chesley, J., et al., 2001. A Detrital Model for the Origin of Gold and Sulfides in the Witwatersrand Basin Based on Re-Os Isotopes. *Geochimica et Cosmochimica Acta*, 65(13): 2149–2159. doi:10.1016/s0016-7037(01)00588-9

Lentz, D. R., Suzuki, K., 2000. A Low F Pegmatite-Related Mo Skarn from the Southwestern Grenville Province, Ontario, Canada: Phase Equilibria and Petrogenetic Implications. *Economic Geology*, 95(6): 1319–1337. doi:10.2113/95.6.1319

Levresse, G., Cheilletz, A., Gasquet, D., et al., 2004. Osmium, Sulphur, and Helium Isotopic Results from the Giant Neoproterozoic Epithermal Imiter Silver Deposit, Morocco: Evidence for a Mantle Source. *Chemical Geology*, 207(1/2): 59–79. doi:10.1016/j.chemgeo.2004.02.004

Li, N., Chen, Y. J., Santosh, M., et al., 2011. The 1.85 Ga Mo Mineralization in the Xiong'er Terrane, China: Implications for Metallogeny Associated with Assembly of the Columbia Supercontinent. *Precambrian Research*, 186(1–4): 220–232. doi:10.1016/j.precamres.2011.01.019

Li, W. C., Zeng, P. S., Hou, Z. Q., et al., 2011. The Pulang Porphyry Copper Deposit and Associated Felsic Intrusions in Yunnan Province, Southwest China. *Economic Geology*, 106(1): 79–92. doi:10.2113/econgeo.106.1.79

Liu, C., Deng, J. F., Kong, W. Q., et al., 2011. LA-ICP-MS Zircon U-Pb Geochronology of the Fine-Grained Granite and Molybdenite Re-Os Dating in the Wurinitu Molybdenum Deposit, Inner Mongolia, China. *Acta Geologica Sinica—English Edition*, 85(5): 1057–1066. doi:10.1111/j.1755-6724.2011.00240.x

Liu, X. F., Yuan, S. D., Wu, S. H., 2012. Re-Os Dating of the Molybdenite from the Jinchuantang Tin-Bismuth Deposit in Hunan Province and Its Geological Significance. *Acta Petrologica Sinica*, 28(1): 39–51. doi:10.1007/s12583-015-0539-6 (in Chinese with English Abstract)

Liu, Y. Y., Qi, L., Gao, J. F., et al., 2015. Re-Os Dating of Galena and Sphalerite from Lead-Zinc Sulfide Deposits in Yunnan Province, SW China. *Journal of Earth Science*, 25(3): 343–351. doi:10.1007/s12583-015-0539-6

Lü, L. S., Mao, J. W., Li, H. B., et al., 2011. Pyrrhotite Re-Os and

SHRIMP Zircon U-Pb Dating of the Hongqiling Ni-Cu Sulfide Deposits in Northeast China. *Ore Geology Reviews*, 43(1): 106–119. doi:10.1016/j.oregeorev.2011.02.003

Lu, Y. F., Ma, L. Y., Qu, W. J., et al., 2006. U-Pb and Re-Os Isotope Geochronology of Baoshan Cu-Mo Polymetallic Ore Deposit in Hunan Province. *Acta Petrologica Sinica*, 22(10): 2483–2492 (in Chinese with English Abstract)

Mallmann, G., O'Neill, H. S. C., 2007. The Effect of Oxygen Fugacity on the Partitioning of Re between Crystals and Silicate Melt during Mantle Melting. *Geochimica et Cosmochimica Acta*, 71(11): 2837–2857. doi:10.1016/j.gca.2007.03.028

Mao, J. W., Zhang, Z. H., Zhang, Z. C., et al., 1999. Re-Os Age Dating of Molybdenites in the Xiaoliugou Tungsten Deposit in the Northern Qilian Mountains and Its Significance. *Geological Review*, 45(4): 412–417 (in Chinese with English Abstract)

Mathur, R., Marschik, R., Ruiz, J., et al., 2002. Age of Mineralization of the Candelaria Fe Oxide Cu-Au Deposit and the Origin of the Chilean Iron Belt, Based on Re-Os Isotopes. *Economic Geology*, 97(1): 59–71. doi:10.2113/gsecongeo.97.1.59

Mathur, R., Ruiz, J., Titley, S., et al., 2000. Different Crustal Sources for Au-Rich and Au-Poor Ores of the Grasberg Cu-Au Porphyry Deposit. *Earth and Planetary Science Letters*, 183(1/2): 7–14. doi:10.1016/s0012-821x(00)00256-9

Mathur, R., Ruiz, J., Tornos, F., 1999. Age and Sources of the Ore at Tharsis and Rio Tinto, Iberian Pyrite Belt, from Re-Os Isotopes. *Mineralium Deposita*, 34(8): 790–793. doi:10.1007/s001260050239

Mavrogenes, J. A., MacIntosh, I. W., Ellis, D. J., 2001. Partial Melting of the Broken Hill Galena-Sphalerite Ore: Experimental Studies in the System PbS-FeS-ZnS-(Ag_2S). *Economic Geology*, 96(1): 205–210. doi:10.2113/gsecongeo.96.1.205

Meisel, T., Moser, J., Wegscheider, W., 2001. Recognizing Heterogeneous Distribution of Platinum Group Elements (PGE) in Geological Materials by Means of the Re-Os Isotope System. *Fresenius Journal of Analytical Chemistry*, 370(5): 566–572. doi:10.1007/s002160100791

Meisel, T., Walker, R. J., Morgan, J. W., 1996. The Osmium Isotopic Composition of the Earth's Primitive Upper Mantle. *Nature*, 383(6600): 517–520. doi:10.1038/383517a0

Melfos, V., Voudouris, P., Arikas, K. et al., 2001. Rhenium-Rich Molybdenites in Thracian Porphyry Cu±Mo Occurrences, NE Greece. *Bulletin of the Geological Society of Greece*, 34: 1015–1022 (in Greek with English Abstract)

Morelli, R. M., Bell, C. C., Creaser, R. A., et al., 2010. Constraints on the Genesis of Gold Mineralization at the Homestake Gold Deposit, Black Hills, South Dakota from Rhenium-Osmium Sulfide Geochronology. *Mineralium Deposita*, 45(5): 461–480. doi:10.1007/s00126-010-0284-9

Morelli, R. M., Creaser, R. A., Selby, D., et al., 2004. Re-Os Sulfide Geochronology of the Red Dog Sediment-Hosted Zn-Pb-Ag Deposit, Brooks Range, Alaska. *Economic Geology*, 99(7): 1569–1576. doi:10.2113/gsecongeo.99.7.1569

Morelli, R. M., Creaser, R. A., Selby, D., et al., 2005. Rhenium-Osmium Geochronology of Arsenopyrite in Meguma Group Gold Deposits, Meguma Terrane, Nova Scotia, Canada: Evidence for Multiple Gold-Mineralizing Events. *Economic Geology*, 100(6): 1229–1242. doi:10.2113/gsecongeo.100.6.1229

Nozaki, T., Kato, Y., Suzuki, K., 2010. Re-Os Geochronology of the Iimori Besshi-Type Massive Sulfide Deposit in the Sanbagawa Metamorphic Belt, Japan. *Geochimica et Cosmochimica Acta*, 74(15): 4322–4331. doi:10.1016/j.gca.2010.04.055

Pruseth, K. L., Jehan, N., Sahu, P., et al., 2014. The Possibility of a ZnS-Bearing Sulfide Melt at 600 ºC: Evidence from the Rajpura-Dariba Deposit, India, Supported by Laboratory Melting Experiment. *Ore Geology Reviews*, 60: 50–59. doi:10.1016/j.oregeorev.2013.12.012

Qi, L., Gao, J. F., Zhou, M. F., et al., 2013. The Design of Re-Usable Carius Tubes for the Determination of Rhenium, Osmium and Platinum-Group Elements in Geological Samples. *Geostandards and Geoanalytical Research*, 37(3): 345–351. doi:10.1111/j.1751-908x.2012.00211.x

Qi, L., Zhou, M. F., Gao, J. F., 2010. An Improved Carius Tube Technique for Determination of Low Concentrations of Re and Os in Pyrites. *Journal of Analytical Atomic Spectrometry*, 25(4): 585. doi:10.1039/b919016c

Reisberg, L., Meisel, T., 2002. The Re-Os Isotopic System: A Review of Analytical Techniques. *Geostandards and Geoanalytical Research*, 26(3): 249–267. doi:10.1111/j.1751-908x.2002.tb00633.x

Righter, K., Chesley, J. T., Geist, D., et al., 1998. Behavior of Re during Magma Fractionation: An Example from Volcan Alcedo, Galapagos. *Journal of Petrology*, 39(4): 785–795. doi:10.1093/petroj/39.4.785

Sattari, P., Brenan, J. M., Horn, I., et al., 2002. Experimental Constraints on the Sulfide- and Chromite-Silicate Melt Partitioning Behavior of Rhenium and Platinum-Group Elements. *Economic Geology*, 97(2): 385–398. doi:10.2113/gsecongeo.97.2.385

Selby, D., Creaser, R. A., 2004. Macroscale NTIMS and Microscale LA-MC-ICP-MS Re-Os Isotopic Analysis of Molybdnite: Testing Spatial Restrictions for Reliable Re-Os Age Determinations, and Implications for the Decoupling of Re and Os within Molybdenite. *Geochimica et Cosmochimica Acta*, 68(19): 3897–3908

Selby, D., Kelley, K. D., Hitzman, M. W., et al., 2009. Re-Os Sulfide (Bornite, Chalcopyrite, and Pyrite) Systematics of the Carbonate-Hosted Copper Deposits at Ruby Creek, Southern Brooks Range, Alaska. *Economic Geology*, 104(3): 437–444. doi:10.2113/gsecongeo.104.3.437

Sharp, W. E., 1969. Melting Curves of Sphalerite, Galena, and Pyrrhotite and the Decomposition Curve of Pyrite between 30 and 65 Kilobars. *Journal of Geophysical Research*, 74(6): 1645–1652. doi:10.1029/jb074i006p01645

Si, R. J., 2006. Ore Deposit Geochemistry of the Fule Dispersed Element-Polymetallic Deposit, Yunnan Province: [Dissertation]. Institute of Geochemistry, Chinese Academy of Sciences, Guiyang. 1–121 (in Chinese with English Abstract)

Song, G. X., Qin, K. Z., Li, G. M., et al., 2012.

Geochronologic and Isotope Geochemical Constraints on Magmatism and Associated W-Mo Mineralization of the Jitoushan W-Mo Deposit, Middle–Lower Yangtze Valley. *International Geology Review*, 54(13): 1532–1547. doi:10.1080/00206814.2011.646806

Spry, P. G., Mathur, R. D., Bonsall, T. A., et al., 2014. Re-Os Isotope Evidence for Mixed Source Components in Carbonate-Replacement Pb-Zn-Ag Deposits in the Lavrion District, Attica, Greece. *Mineralogy and Petrology*, 108(4): 503–513. doi:10.1007/s00710-013-0314-2

Spry, P. G., Plimer, I. R., Teale, G. S., 2008. Did the Giant Broken Hill (Australia) Zn-Pb-Ag Deposit Melt? *Ore Geology Reviews*, 34(3): 223–241. doi:10.1016/j.oregeorev.2007.11.001

Stein, H. J., 2006. Low-Rhenium Molybdenite by Metamorphism in Northern Sweden: Recognition, Genesis, and Global Implications. *Lithos*, 87(3/4): 300–327. doi:10.1016/j.lithos.2005.06.014

Stein, H. J., Markey, R. J., Morgan, J. W., et al., 2001. The Remarkable Re-Os Chronometer in Molybdenite: How and why It Works. *Terra Nova*, 13(6): 479–486. doi:10.1046/j.1365-3121.2001.00395.x

Stein, H. J., Morgan, J. W., Schersten, A., 2000. Re-Os Dating of Low-Level Highly Radiogenic (LLHR) Sulfides: The Harnas Gold Deposit, Southwest Sweden, Records Continental-Scale Tectonic Events. *Economic Geology*, 95(8): 1657–1671. doi:10.2113/gsecongeo.95.8.1657

Stevens, G., Prinz, S., Rozendaal, A., 2005. Partial Melting of the Assemblage Sphalerite+Galena+Pyrrhotite+Chalcopyrite+Sulfur: Implications for High-Grade Metamorphosed Massive Sulfide Deposits. *Economic Geology*, 100(4): 781–786. doi:10.2113/100.4.781

Suzuki, K., Shimizu, H., Masuda, A., 1996. Re-Os Dating of Molybdenites from Ore Deposits in Japan: Implication for the Closure Temperature of the Re-Os System for Molybdenite and the Cooling History of Molybdenum Ore Deposits. *Geochimica et Cosmochimica Acta*, 60(16): 3151–3159

Taghipour, N., Aftabi, A., Mathur, R., 2008. Geology and Re-Os Geochronology of Mineralization of the Miduk Porphyry Copper Deposit, Iran. *Resource Geology*, 58(2): 143–160. doi:10.1111/j.1751-3928.2008.00054.x

Wang, L., Hu, M. A., Yang, Z., et al., 2011. U-Pb and Re-Os Geochronology and Geodynamic Setting of the Dabaoshan Polymetallic Deposit, Northern Guangdong Province, South China. *Ore Geology Reviews*, 43(1): 40–49. doi:10.1016/j.oregeorev.2011.06.008

Xie, G. Q., Mao, J. W., Zhao, H. J., et al., 2011. Timing of Skarn Deposit Formation of the Tonglushan Ore District, Southeastern Hubei Province, Middle–Lower Yangtze River Valley Metallogenic Belt and its Implications. *Ore Geology Reviews*, 43(1): 62–77. doi:10.1016/j.oregeorev.2011.05.005

Xiong, Y. L., Wood, S. A., 1999. Experimental Determination of the Solubility of ReO_2 and the Dominant Oxidation State of Rhenium in Hydrothermal Solutions. *Chemical Geology*, 158(3/4): 245–256. doi:10.1016/s0009-2541(99)00050-9

Xiong, Y. L., Wood, S. A., 2002. Experimental Determination of the Hydrothermal Solubility of ReS_2 and the Re-ReO_2 Buffer Assemblage and Transport of Rhenium under Supercritical Conditions. *Geochemical Transactions*, 3(1): 1–10

Xiong, Y., Wood, S., Kruszewski, J., 2006. Hydrothermal Transport and Deposition of Rhenium under Subcritical Conditions Revisited. *Economic Geology*, 101(2): 471–478. doi:10.2113/gsecongeo.101.2.471

Xiong, Y., Wood, S. A., 2001. Hydrothermal Transport and Deposition of Rhenium under Subcritical Conditions (up to 200 ºC) in Light of Experimental Studies. *Economic Geology*, 96(6): 1429–1444. doi:10.2113/gsecongeo.96.6.1429

Ye, L., Gao, W., Yang, Y. L., 2012. Trace Elements in Sphalerite in Laochang Pb-Zn Polymetallic Deposit, Lancang, Yunnan Province. *Acta Petrologica Sinica*, 28(5): 1362–1372 (in Chinese with English Abstract)

Yu, G., Yang, G., Chen, J. F., et al., 2005. Re-Os Dating of Gold-Bearing Arsenopyrite of the Maoling Gold Deposit, Liaoning Province, Northeast China and Its Geological Significance. *Chinese Science Bulletin*, 50(14): 1509. doi:10.1360/04wd0229

Zeng, P. S., Hou, Z. Q., Wang, H. P., et al., 2004. Re-Os Dating of the Pulang Porphyry Copper Deposit in Zhongdian, NW Yunnan, and Its Geological Significance. *Acta Geologica Sinica—English Edition*, 78: 604–609. doi:10.1111/j.1755-6724.2004.tb00172.x

Zeng, Q. D., Chu, S. X., Liu, J. M., et al., 2012. Mineralization, Alteration, Structure, and Re-Os Age of the Lanjiagou Porphyry Mo Deposit, North China Craton. *International Geology Review*, 54(10): 1145–1160. doi:10.1080/00206814.2011.626575

Zhang, F., Liu, S. W., Li, Q. G., et al., 2011. Re-Os and U-Pb Geochronology of the Erlihe Pb-Zn Deposit, Qinling Orogenic Belt, Central China, and Constraints on Its Deposit Genesis. *Acta Geologica Sinica—English Edition*, 85(3): 673–682

Zhang, J. W., Zhu, C. M., Luo, T. Y., et al., 2015. Sn-Bearing Capability Studies of Basaltic and Granitic Magma from the Gejiu tin Deposit: Evidence from High Temperature and High Pressure Petrological Experimentation. *Acta Mineralogica Sinica*, 35(2): 159–166 (in Chinese with English Abstract)

Zhu, Z. M., Sun, Y. L., 2013. Direct Re-Os Dating of Chalcopyrite from the Lala IOCG Deposit in the Kangdian Copper Belt, China. *Economic Geology*, 108(4): 871–882

Zimmerman, A., Stein, H. J., Hannah, J. L., et al., 2008. Tectonic Configuration of the Apuseni-Banat-Timok-Srednogorie Belt, Balkans-South Carpathians, Constrained by High Precision Re-Os Molybdenite Ages. *Mineralium Deposita*, 43(1): 1–21